# Contribution of Electrostatics to the Binding of Pancreatic-Type Ribonucleases to Membranes

Nadia K. Sundlass,[†] Chelcie H. Eller,[‡] Qiang Cui,[§] and Ronald T. Raines*[,‡,§]

[†]Medical Scientist Training Program and Graduate Program in Biophysics, [‡]Department of Biochemistry, and [§]Department of Chemistry, University of Wisconsin−Madison, Madison, Wisconsin 53706, United States

ABSTRACT: Pancreatic-type ribonucleases show clinical promise as chemotherapeutic agents but are limited in efficacy by the inefficiency of their uptake by human cells. Cellular uptake can be increased by the addition of positive charges to the surface of ribonucleases, either by site-directed mutagenesis or by chemical modification. This observation has led to the hypothesis that ribonuclease uptake by cells depends on electrostatics. Here, we use a combination of experimental and computational methods to ascertain the contribution of electrostatics to the cellular uptake of ribonucleases. We focus on three homologous ribonucleases: Onconase (frog), ribonuclease A (cow), and ribonuclease 1 (human). Our results support the hypothesis that electrostatics are necessary for the cellular uptake of Onconase. In contrast, specific interactions with cell-surface components likely contribute more to the cellular uptake of ribonuclease A and ribonuclease 1 than do electrostatics. These findings provide insight for the design of new cytotoxic ribonucleases.
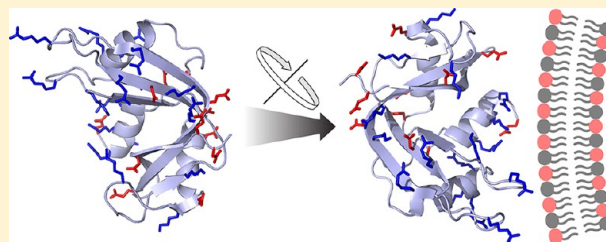
Bovine pancreatic ribonuclease (RNase A; E.C. 3.1.27.5) has been the object of much seminal research in biochemistry and related fields.[1−3] The impact of this small secretory enzyme expanded when some members of the pancreatic-type ribonuclease superfamily were found to be natural toxins for tumor cells,[4−8] and others were engineered to be cytotoxic.[9,10] Notably, a ribonuclease from the northern leopard frog (*Rana pipiens*), known as "Onconase" (ONC or ranpirnase), was granted both fast track and orphan drug status from the FDA for the treatment of malignant mesothelioma. Ultimately, however, dose-limiting renal toxicity limited its clinical utility.[5] More promising are cytotoxic variants of mammalian ribonucleases, such as RNase A and its human homologue (RNase 1), which demonstrate selective cytotoxicity without renal accumulation.[6,11]

A cytotoxic ribonuclease must be internalized by tumor cells, translocate across the endosomal membrane to the cytosol, evade the cytosolic ribonuclease inhibitor protein (RI), and catalyze the degradation of RNA.[9] RI is a 50 kDa cytosolic protein that binds to some ribonucleases, inhibiting their ribonucleolytic activity.[12] ONC does not bind to human RI under physiological conditions[13] and is naturally cytotoxic to human cells. Conversely, wild type RNase A and wild type RNase 1 bind to RI with femtomolar affinity and are not cytotoxic.[14,15] Variants engineered to evade RI do, however, demonstrate cytotoxicity.[9,10,15−18]

Inefficient cellular internalization can limit the cytotoxic activity of a pancreatic-type ribonuclease.[9] For example, ribonucleases exhibit picomolar IC_{50} values when injected directly into the cytosol but micromolar IC_{50} values when simply incubated with cells.[19] Although ONC has been proposed to bind to two saturable sites on 9L glioma cells with K_d values of 0.25 μM and 62 nM,[20] ONC demonstrates nonsaturable binding to HeLa, K-562, and CHO cells.[21−23] ONC and its homologues are highly cationic proteins (Figure 1), and their endocytosis occurs via nonreceptor-mediated pathways[21] similar to those used by cationic cell-penetrating peptides.[24]

Increasing the endocytosis of a ribonuclease can increase its cytotoxicity. For example, the covalent conjugation of RNase A to transferrin, which does have a cell-surface receptor, increases both its cellular uptake and cytotoxic activity.[25] In addition, increasing the net positive charge of RNase A and RNase 1 through either site-directed mutagenesis or chemical modification increases endocytosis.[26−28] Likewise, decreasing the net negative charge of mammalian cells decreases the uptake of RNase A and ONC.[23] Accordingly, the endocytosis of ribonucleases is likely mediated by electrostatic forces.[29] In addition to providing affinity, electrostatic forces could also contribute to the therapeutic index of pancreatic-type ribonucleases because cancer cells tend to be more anionic than analogous noncancerous cells.[30−32]

Ribonuclease cytotoxicity relies on translocation into the cytosol.[7] RNase A is found in lysosomes 100 h after endocytosis, consistent with inefficient translocation to the cytosol.[33] Indeed, only ∼7% of the RNase A molecules that enter a cell reach the cytosol in 24 h.[34] Neutralization of the pH in endosomes results in an increase in ONC cytotoxicity, presumably due to increased translocation.[35] Cytotoxicity has also been found to correlate with the ability of a ribonuclease to disrupt synthetic anionic membranes.[36]

We suspected that theoretical approaches could provide insight on the interaction between ribonucleases and cellular membranes. In particular, we reasoned that a numerical solution of the Poisson−Boltzmann (PB) equation could be used to calculate the interaction energy between molecules using
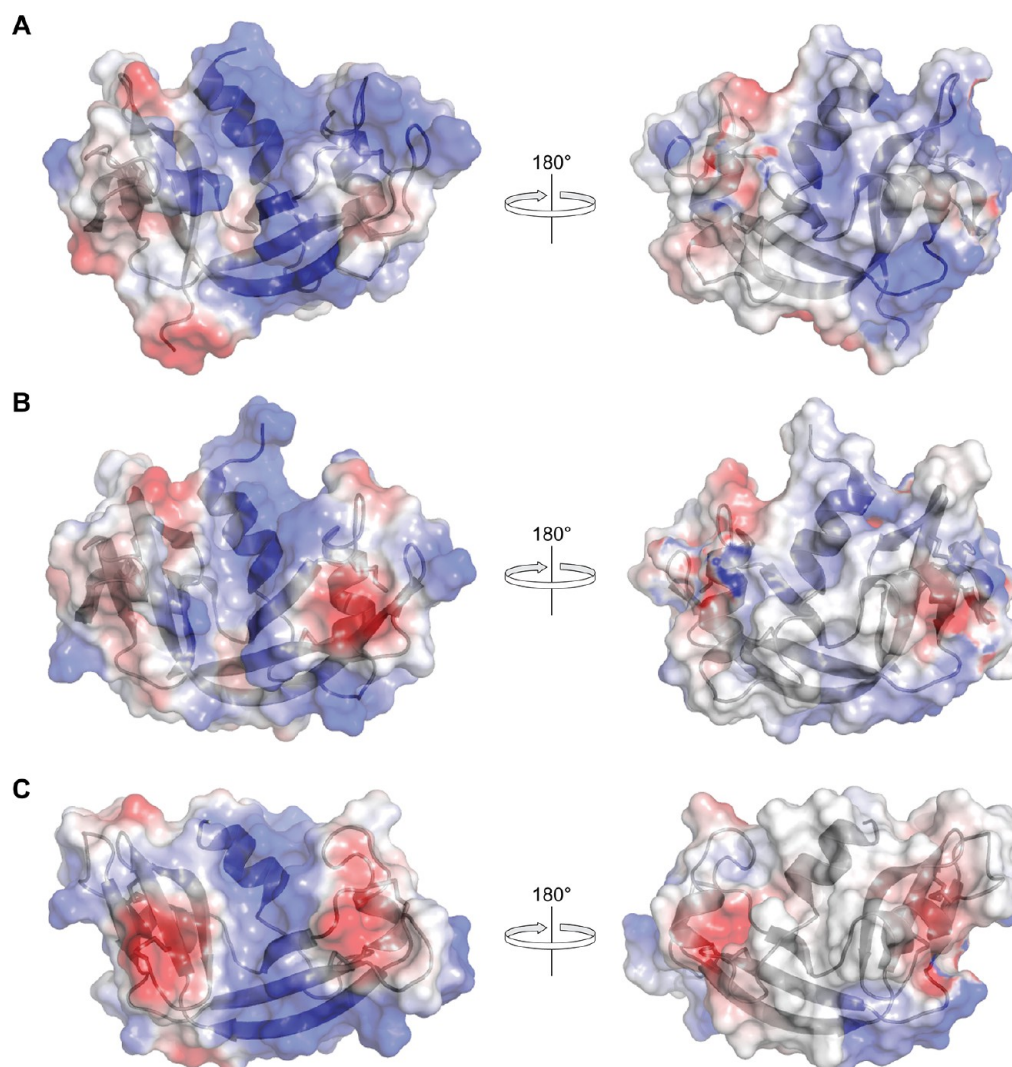
Figure 1. Electrostatic surface potential of pancreatic-type ribonucleases. (A) RNase 1 (1Z7X), which has a net charge (Arg + Lys − Asp − Gly) of $Z = +6$. (B) RNase A (1KF5), which has $Z = +4$ and a 68% sequence identity with RNase 1. (C) ONC (1ONC), which has $Z = +5$ and a 23% sequence identity with RNase 1. Images were made with the program PyMOL from Schrödinger (Portland, OR).

continuum electrostatics. The PB approach has been used to calculate the binding energy between rigid proteins and model membranes and to identify energetically favorable orientations for binding.[37] Of special relevance was the use of PB calculations to predict the orientation of membrane-bound dimeric ribonucleases.[36] These calculations indicated that the ensuing electrostatic energy correlates with both the ability to disrupt membranes and cytotoxicity. The PB-based computational framework does not describe effects due to the atomic nature of solvent and lipid molecules but is particularly useful in the current study, which aims to probe the contribution from generic electrostatic effects to the binding of a protein to anionic membranes.

Here, we use computational and experimental approaches to measure the contribution of electrostatics to the binding of RNase 1, RNase A, and ONC to anionic membranes. We report on the effect of salt concentration on the formation of a protein−membrane complex. We then use computational analysis to reveal favorable orientations for those complexes and to highlight differences caused by the differential distribution of charges on the surface of RNase 1, RNase A, and ONC. Finally, we compare experimental binding measurements to PB calculations and

simulations using an implicit membrane model supplemented with a Gouy−Chapman term (IMM1−GC), which is another electrostatics-driven approach. The comparison highlights the advantages of each computational method and the quality of their predictions. Together, the experimental and computational data indicate that, despite similar structures and net charges, homologous ribonucleases have distinct affinities for anionic surfaces.

■ MATERIALS AND METHODS

Materials. BODIPY FL *N*-(2-aminoethyl)maleimide (catalog number B-10250) was from Molecular Probes (Carlsbad, CA). 1,2-Dioleoyl-*sn*-glycero-3-phospho-L-serine (DOPS) and 1,2-dioleoyl-*sn*-glycero-3-phosphocholine (DOPC) were from Avanti Polar Lipids (Alabaster, AL). All other chemicals used were of commercial grade or better and were used without further purification.

Analytical Instruments. Molecular mass was measured by MALDI-TOF mass spectrometry using a Voyager-DE-PRO Biospectrometry Workstation from Applied Biosystems (Foster City, CA). Fluorescence was quantified with an Infinite M1000 plate reader from Tecan (Männedorf, Switzerland).

Production of Fluorescently Labeled Ribonucleases. P19C RNase 1,[29] A19C RNase A,[38] and S61C ONC,[22] which are variants with an orphan cysteine residue, were prepared as described previously. The free cysteine residue in these variants was protected as a mixed disulfide by reaction with 5,5′-dithio-bis(2-nitrobenzoic acid). Prior to fluorophore attachment, each mixed disulfide was reduced with dithiothreitol (5 equiv) then desalted by using a PD-10 desalting column from GE Biosciences (Piscataway, NJ). Deprotected proteins were reacted for 4−6 h at 25 °C in PBS with BODIPY FL N-(2-aminoethyl)maleimide (10 equiv) in DMSO. The reaction was quenched by rapid dilution into 50 mM sodium acetate buffer at pH 5.0. Conjugates were purified by chromatography using a HiTrap SPHP column, and concentrations of conjugates were determined with a bicinchoninic acid assay kit from Pierce (Rockford, IL).

Liposome Formation. Large unilamellar vesicles (i.e., liposomes) were formed by mixing DOPC and DOPS solvated by chloroform in a 3:2 molar ratio at a 5 mM concentration of total lipid. The lipids were dried under $N_2(g)$ to remove the chloroform, then dried further under vacuum overnight. The lipids were resuspended in 20 mM Tris−HCl buffer at pH 7.0, containing NaCl (50 or 80 mM), by vortexing and were then allowed to hydrate for 1 h at 37 °C. The vesicles were then extruded 19 times through a 100 nm filter to form liposomes that were ~130 nm in diameter according to dynamic light scattering data obtained with an N4-Plus instrument from Beckman Coulter (Brea, CA).

Liposome−Ribonuclease Binding Assay. Fluorescence polarization was used to measure the binding affinity of the fluorescently labeled ribonucleases to liposomes. A concentration range (4.5 mM → 2.25 nM; 2-fold dilutions) of liposomes was incubated with BODIPY-labeled ribonuclease (50 nM) in 20 mM Tris−HCl buffer at pH 7.0, containing NaCl (50 or 80 mM), for 1 h at 23 °C while shaking. Then, fluorescence polarization was measured with excitation at 470 nm and emission at 530 nm, and the value of the equilibrium dissociation constant (K_d) was calculated with the equation

$$R = \frac{(R_{max} - R_{min})[\text{lipid}]}{K_d + [\text{lipid}]} \tag{1}$$

where R refers to the observed polarization, R_{max} refers to the polarization when the ribonuclease is bound fully, R_{min} refers to the polarization when the ribonuclease is free, and [lipid] refers to the concentration of DOPS.

Poisson−Boltzmann Calculations. Electrostatic calculations were performed with the program APBS 1.2.1.[39] For the calculations presented herein, the free energy of binding, $\Delta\Delta G_{bind}$, between the protein and membrane was calculated with the equation

$$\Delta\Delta G_{bind} = \Delta\Delta G_{solv} + \Delta\Delta G_{Coul} \tag{2}$$

where $\Delta\Delta G_{solv}$ refers to the contribution of solvation to binding and $\Delta\Delta G_{Coul}$ refers to the Coulombic contribution to binding. The solvation contribution to binding was calculated as

$$\Delta\Delta G_{solv} = \Delta G_{solv,complex} - \Delta G_{solv,protein} - \Delta G_{solv,membrane} \tag{3}$$

where the terms refer to the solvation free energy of the protein−membrane complex, the protein, and the model membrane, respectively. The individual free energy terms were calculated by numerical solution of the Poisson−Boltzmann equation:

$$-\nabla \cdot \varepsilon(\bar{r})\nabla V = \rho_f(\bar{r}) - 2qn_\infty \sinh\left(\frac{qV(\bar{r})}{k_B T}\right) \tag{4}$$

The Coulombic contribution was calculated in analogy to eq 3 as

$$\Delta\Delta G_{Coul} = \Delta G_{Coul,complex} - \Delta G_{Coul,protein}$$
$$- \Delta G_{Coul,membrane} \tag{5}$$

where the terms are the summation of all pairwise Coulombic interactions between all atoms within the protein−membrane complex, the protein, and the model membrane, respectively.

The structures of RNase 1, RNase A, and ONC were derived from PDB entries 1Z7X,[15] 1KF5,[40] and 1ONC,[41] respectively. All water molecules were removed from the PDB file prior to the addition of hydrogen atoms and atomic charges on the basis of the CHARMM 27 forcefield with PDB2PQR.[42−44] The model membrane was approximated by an 80 × 80 Å plane of spheres ($r = 3$ Å, $q = -1$, $\varepsilon = 78.50$) with a charge density of 1 sphere/130 Å². The solvation free energy of the protein was calculated with two levels of focusing calculations in a 400 × 400 × 400 Å box with 0.5 Å spacing at the finest level. Dielectric maps of the system were outputted and altered such that the dielectric constant below the charged plane of spheres was $\varepsilon = 2.0$. These dielectric maps were used to calculate the solvation free energies of the membrane and the protein−membrane complex. The model membrane was placed 5 Å below the bottom of the protein. Conformations of the protein relative to the membrane were sampled by applying a rotation matrix based on Euler's angles ($\theta = 0$, $\phi = 0-2\pi$, $\psi = 0-\pi$) in 15° increments on the protein coordinates.

IMM1−GC Calculations. The IMM1−GC model was used to model an anionic membrane in CHARMM. IMM1−GC is based on the IMM1 model with the addition of a Gouy−Chapman (GC) term to describe the interaction between charged amino acids and the charged bilayer.[45] The IMM1 models the membrane as a low dielectric slab with a smooth transition to the high dielectric solvent. The IMM1 model is based on the EEF1 model for water-soluble proteins,[46] which neutralizes ionic side chains and uses a linear distance-dependent dielectric constant. The solvation free energy for a protein, ΔG_{solv}, is assumed to be the sum of the solvation free energy for individual atoms within the protein.
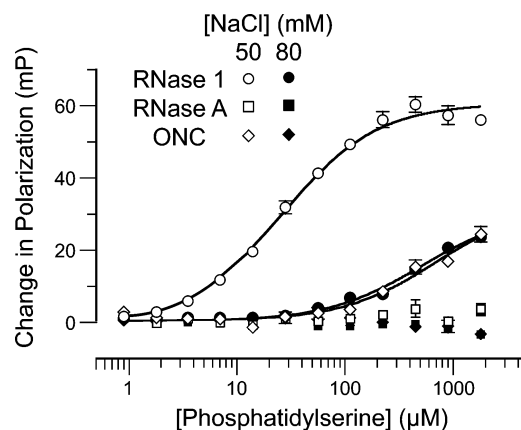

Figure 2. Ribonuclease binding isotherms toward phosphatidylserine liposomes. Binding was measured by fluorescence polarization using fluorescently labeled ribonucleases and increasing the concentration of liposomes containing DOPC and DOPS at a ratio of 3:2 in 20 mM Tris−HCl buffer at pH 7.0, containing NaCl (50 or 80 mM). Data were fitted by a nonlinear regression analysis.

Table 1. Experimental and Calculated Affinity of Ribonucleases for a Phosphatidylserine Membrane[a]

	experimental			calculated
ribonuclease	[NaCl] (mM)	K_d (mM)	ΔG_{bind} (kcal/mol)	ΔG_{bind} (kcal/mol)
RNase 1	50	0.027 ± 0.002	-6.23 ± 0.02	-4.7
RNase 1	80	0.5 ± 0.1	-4.5 ± 0.1	-3.6
RNase A	50	>1.8	>-3.7	-2.8
RNase A	80	>1.8	>-3.7	-2.2
ONC	50	0.7 ± 0.2	-4.3 ± 0.2	-3.1
ONC	80	>1.8	>-3.7	-2.5

[a]Experimental data were determined by fluorescence polarization in 20 mM Tris−HCl buffer at pH 7.0. Calculated data were determined by Poisson−Boltzmann analysis.

The effective energy of the protein in the presence of the membrane is given by

$$W_{\text{IMM1-GC}} = E_{\text{intra}} + \Delta G_{\text{solv}} + E_{\text{GC}} \qquad (6)$$

where E_{intra} is the intramolecular energy of the protein and E_{GC} is the interaction between the partial charges of the protein and the charged lipid bilayer based on the Gouy−Chapman theory for a diffuse electrical bilayer.[47]

The initial coordinates were taken from the same PDB entries used in PB calculations. Six different initial orientations were generated with each one corresponding to the face of a cube containing the ribonuclease. The membrane was placed 3 Å below the bottom of the protein perpendicular to the z-axis. The salt concentration was set to 0.1 M and the anionic fraction of the membrane to 40% to match the experimental fluorescence polarization conditions. Molecular dynamic simulations were performed with CHARMM (c35a1).[48] The backbone atoms were constrained using an rmsd constraint. The structures were equilibrated for 100 ps at 298 K and then run for another 2000 ps. The conformations were stored every 0.5 ps and used to calculate the effective energy of the protein in solvent and in the presence of a membrane. A total of 12 simulations were run for each protein. The average binding energy was calculated as
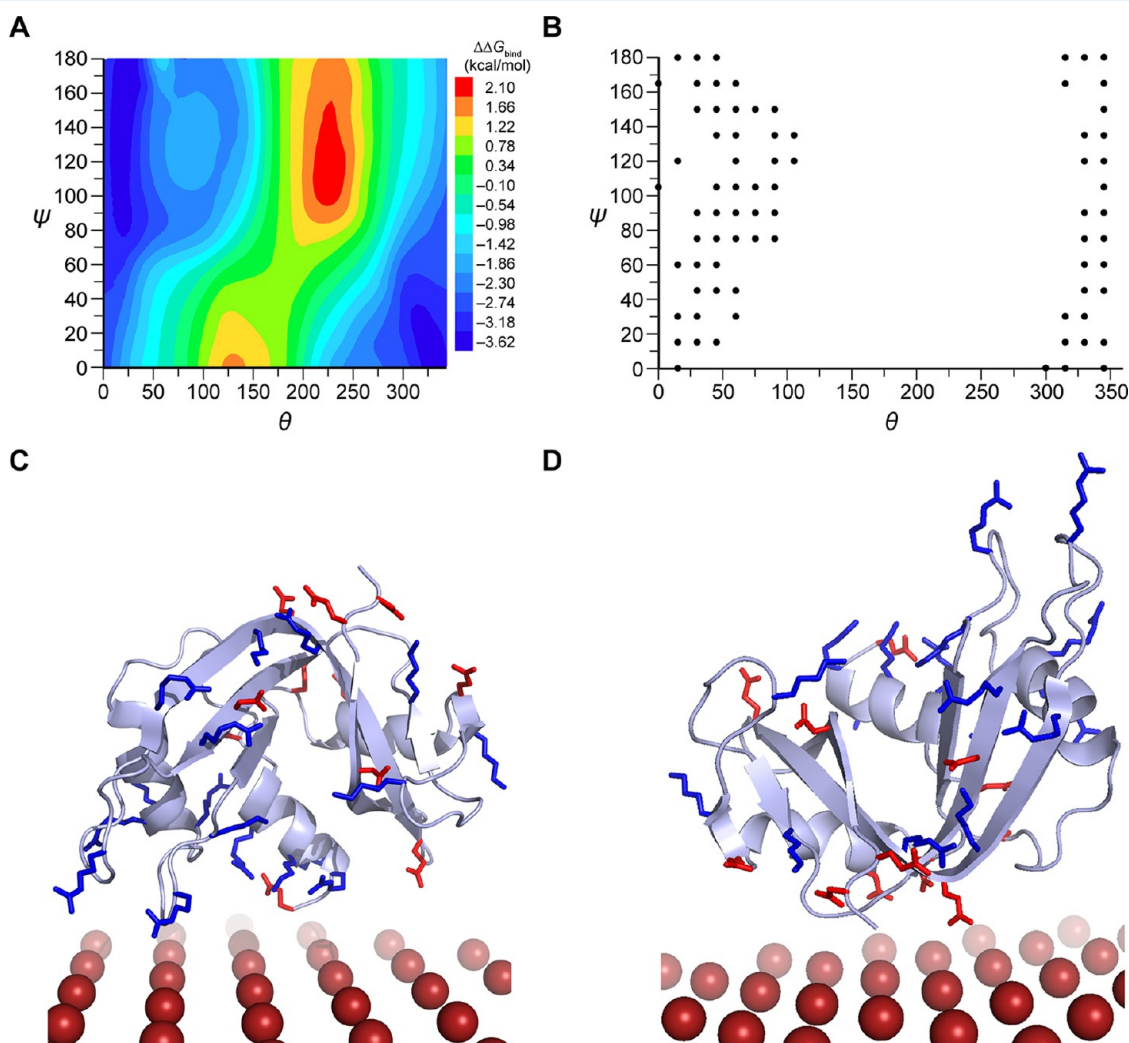

Figure 3. Computational calculation of the binding of RNase 1 to model membranes. (A) Poisson−Boltzmann calculations of the electrostatic free energy of interaction between RNase 1 (PDB entry 1Z7X), rotated using Euler angles ($\theta = 0-360°$, $\psi = 0-180°$, increments of 15°), with a model membrane with an anionic fraction of one electron per 130 Å². (B) Coarse-grained representation of trajectories from a 2 ns IMM1−GC simulation resulting in a protein−membrane complex. Each point represents a snapshot from the trajectory. (C) Depiction of RNase 1 with a model membrane in the most energetically favorable orientation from PB calculations. In the images of Figures 3−5, the N-terminal helix is shown in the center-rear; Arg and Lys (blue) and Asp and Glu (red) side chains are shown explicitly. (D) Depiction of RNase 1 with model membrane in the least energetically favorable orientation from PB calculations.
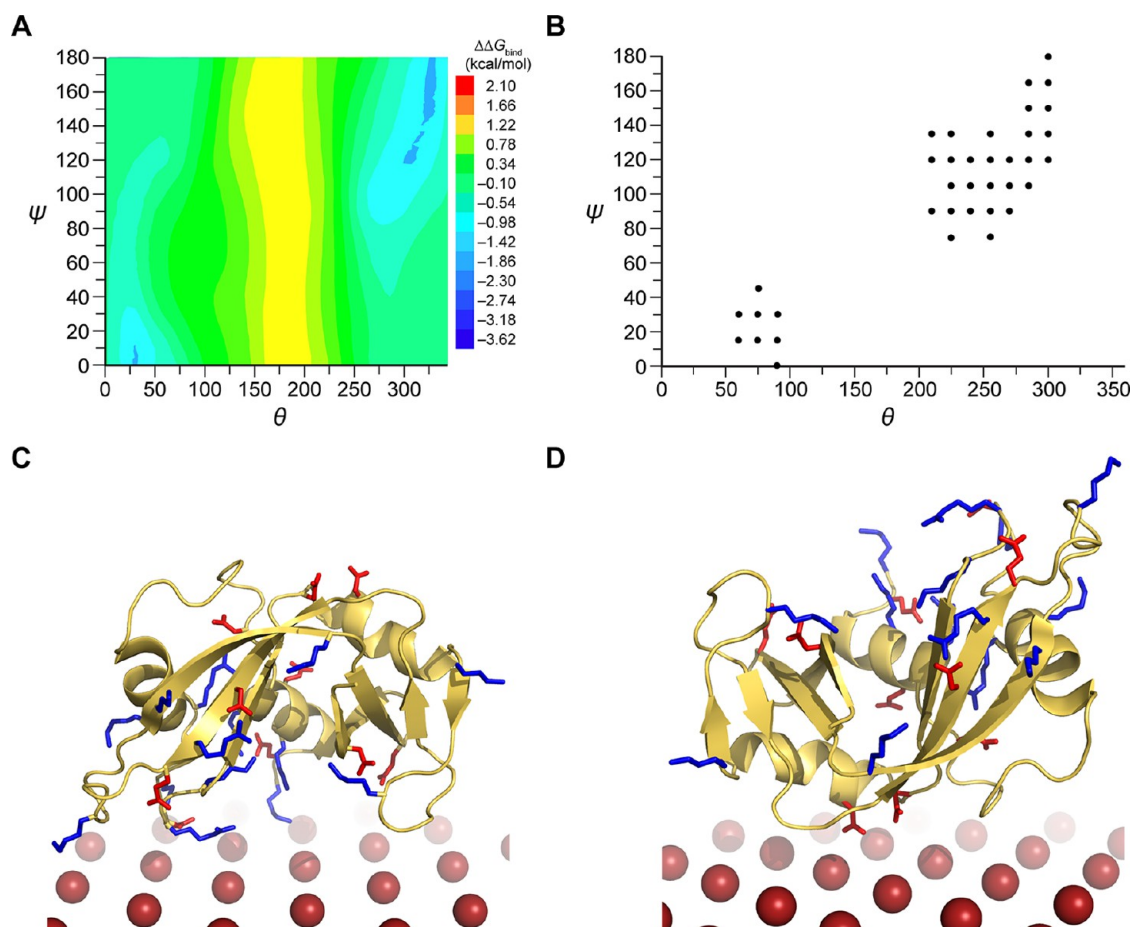
Figure 4. Computational calculation of the binding of RNase A to model membranes. (A) Poisson–Boltzmann calculations of the electrostatic free energy of interaction between RNase A (PDB entry 1KF5), rotated using Euler angles ($\theta = 0-360°$, $\psi = 0-180°$, increments of 15°), with a model membrane with an anionic fraction of one electron per 130 Å^2. (B) Coarse-grained representation of trajectories from a 2 ns IMM1–GC simulation resulting in a protein–membrane complex. (C) Depiction of RNase A with a model membrane in the most energetically favorable orientation from PB calculations. (D) Depiction of RNase A with a model membrane in the least energetically favorable orientation from PB calculations.

the mean binding energy over the last 2 ns of the simulation, and a trajectory was said to bind if the binding free energy was more favorable than −0.8 kcal/mol.

■ RESULTS

Production of Labeled Ribonucleases. Ribonucleases were labeled with BODIPY FL in regions with few cationic residues (residue 19 in both RNase 1 and RNase A and residue 61 in ONC), as these areas were deemed unlikely to interfere with the binding of the ribonucleases to the lipid vesicles. Moreover, the fluorescence of BODIPY is insensitive to pH. The expected mass of purified, labeled proteins was confirmed with MALDI-TOF mass spectrometry, and a properly folded structure was confirmed with measurements of enzymatic activity.[49]

Liposome–Ribonuclease Interactions. The contribution of electrostatics to the cytotoxicity of ribonucleases has been difficult to study. To isolate the first step in the process, we studied the binding of RNase 1, RNase A, and ONC to large unilamellar vesicles containing 40% phosphatidylserine at various salt concentrations. Phosphatidylserine has a net negative charge and normally resides in the cytoplasmic leaflet of the lipid bilayer; in cancerous cells, however, phosphatidylserine relocates to the extracellular leaflet.[31] Cancer cells also display changes in glycosaminoglycans that lead to a more negatively charged surface.[30−32] Hence, we used phosphatidylserine lipo-

somes to mimic the anionic cell surface, providing a comparator for our computational data.

Equilibrium binding isotherms for ribonucleases and liposomes are depicted in Figure 2, and values of K_d are listed in Table 1. RNase A did not bind to the liposomes at either salt concentration. ONC demonstrated some binding in the low salt condition. RNase 1 bound to the liposomes with a K_d value of 27 μM in the low salt condition and with much lower affinity in the high salt condition.

Poisson–Boltzmann Calculations. Poisson–Boltzmann calculations were performed to determine the most favorable orientation for ribonucleases to bind to a model membrane and the binding energy of that orientation (Figures 3–5). The electrostatic map for RNase 1 reveals that the most energetically favorable orientation has its active site facing the membrane (Figures 3A–C). The predicted values of ΔG_{bind} are in gratifying agreement with the experimental ones (Table 1).

Similar to RNase 1, RNase A orients itself so that its active site faces the membrane (Figure 4A–C). This orientation, however, yields a relatively low affinity (Table 1) and is consistent with experiments showing that the binding of RNase A to phosphatidylserine liposomes is not detectable (Figure 2). Interestingly, for both RNase 1 and RNase A, the loops that mediate binding to RI (which is a highly anionic protein[12]) also seem to be important for binding to the model membrane.
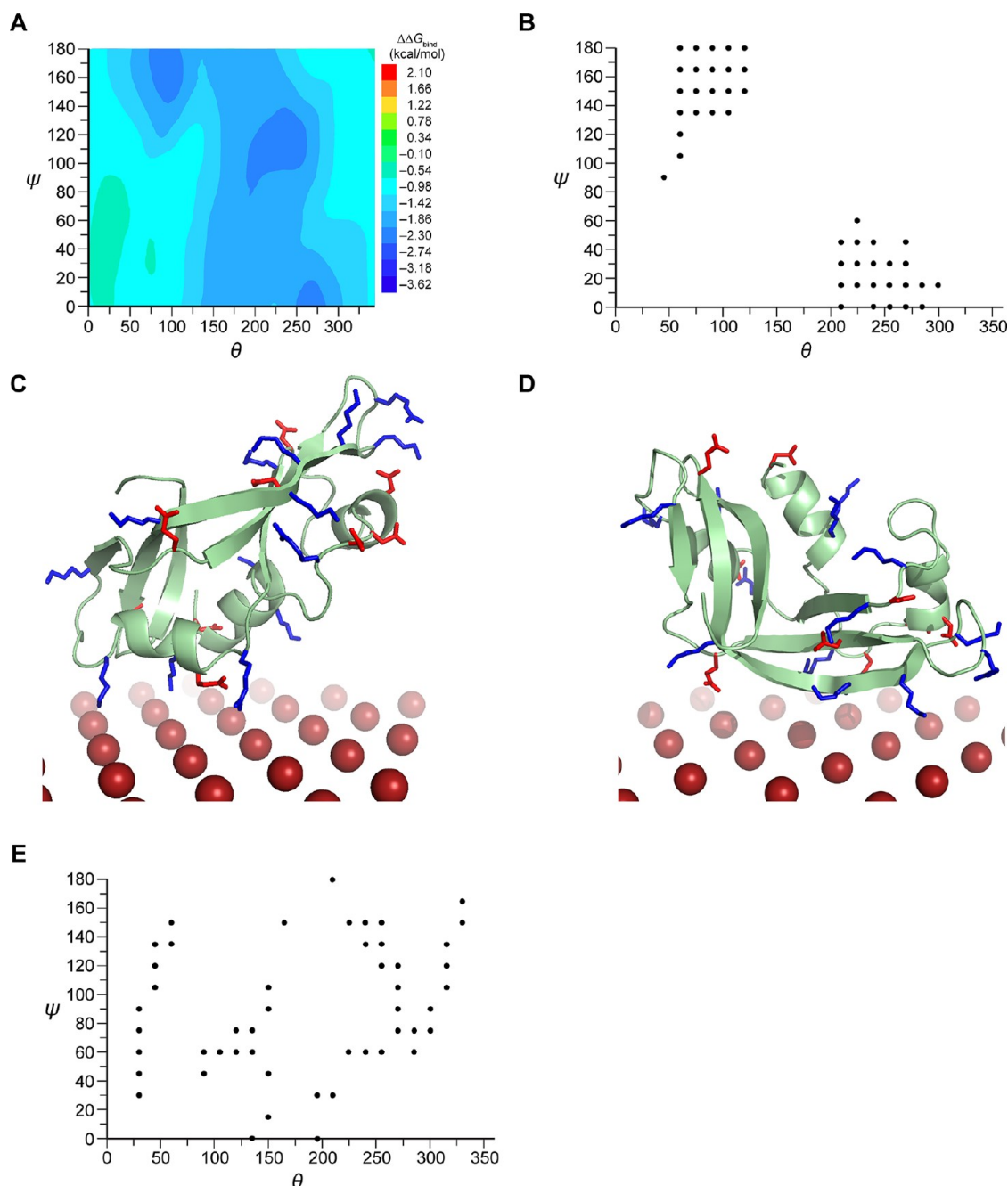
A

B

C

D

E

Figure 5. Computational calculation of ONC binding to model membranes. (A) Poisson−Boltzmann calculations of the electrostatic free energy of interaction between ONC (PDB entry 1ONC), rotated using Euler angles ($\theta = 0−360°$, $\psi = 0−180°$, increments of 15°), with a model membrane with an anionic fraction of one electron per 130 Å^2. (B) A coarse-grained representation of trajectories from a 2 ns IMM1−GC simulation resulting in a protein−membrane complex. (C) Depiction of ONC with a model membrane in the most energetically favorable orientation from PB calculations. (D) Depiction of ONC with a model membrane in the least energetically favorable orientation from PB calculations. (E) Coarse-grained representation of trajectories from a 2 ns IMM1−GC simulation not resulting in a protein−membrane complex.

In contrast to RNase 1 and RNase A, PB calculations predict that ONC can bind favorably either with its active site facing the membrane or in the opposite orientation (Figure 5A−C), which is a highly repulsive orientation for the mammalian ribonucleases. Moreover, ONC appears to be weakly attractive in any orientation, and the most favorable orientation for ONC is only 3-fold more likely than a random orientation. Like RNase A, however, ONC is predicted to bind with low overall affinity in the high salt condition, consistent with experimental data (Table 1).

In general, the PB calculations were more predictive of the affinity of ribonucleases for membranes in the high salt condition than in the low salt condition. For example, the calculated binding free energy for RNase 1 in the low salt condition corresponds to a K_d value of 350 μM, but the experimental K_d value was 27 μM (Table 1). Similarly, ONC is calculated to have a K_d value of ∼8 mM in low salt conditions, but the experimental K_d value was 0.7 mM. Lastly, although RNase A should display affinity only slightly less than that of ONC, its binding was not detectable by experiment. Nevertheless, the predicted trends in the affinity of the proteins for the model membrane, RNase 1 ≫ ONC > RNase A, were qualitatively consistent with the experiment in the low salt condition.

IMM1−GC Simulations. Although the PB calculation results compared well overall with experimental values, especially in the high salt condition, they did not allow for side-chain rearrangements or measure hydrophobic interactions. Hence, we performed multiple short molecular dynamic simulations using the IMM1−GC model. In the simulations, the main chain was constrained, but side chains were unconstrained and the protein was allowed to rotate and translate. For ONC, because the PB calculation did not predict a favorite or an unfavorable orientation, we were surprised to see that only 7 of the 12 trajectories resulted in binding, although the average binding free energies were comparable to those from the PB calculations. The standard deviations reported in Table 2 report on the amount of protein

Table 2. Summary of IMM1−GC Simulations[a]

ribonuclease	starting orientation	binding energy (kcal/mol)
RNase 1	$\theta = 0; \psi = 0$	0.0
		0.0
	$\theta = 180; \psi = 0$	-3.9 ± 0.9
		-4.4 ± 0.7
	$\theta = 270; \psi = 0$	-0.1 ± 0.6
		-2.2 ± 1.5
	$\theta = 270; \psi = 90$	-3.4 ± 0.9
		-3.4 ± 0.7
	$\theta = 90; \psi = 0$	-3.3 ± 0.9
		-4.0 ± 0.8
	$\theta = 90; \psi = 90$	-3.2 ± 1.0
		-3.0 ± 1.2
RNase A	$\theta = 0; \psi = 0$	-0.6 ± 0.9
		-2.2 ± 0.7
	$\theta = 180; \psi = 0$	-2.9 ± 0.5
		-2.6 ± 0.6
	$\theta = 270; \psi = 0$	0.0
		-0.1 ± 0.3
	$\theta = 270; \psi = 90$	-1.1 ± 1.3
		-2.5 ± 0.6
	$\theta = 90; \psi = 0$	-2.1 ± 0.7
		-1.6 ± 1.0
	$\theta = 90; \psi = 90$	-1.8 ± 0.8
		-1.3 ± 0.9
ONC	$\theta = 0; \psi = 0$	-2.0 ± 0.5
		-2.5 ± 0.7
	$\theta = 180; \psi = 0$	-1.5 ± 0.7
		-2.0 ± 0.6
	$\theta = 270; \psi = 0$	-1.5 ± 1.2
		-2.6 ± 0.4
	$\theta = 270; \psi = 90$	-0.2 ± 0.4
		-0.8 ± 0.8
	$\theta = 90; \psi = 0$	0.0
		-0.1 ± 0.3
	$\theta = 90; \psi = 90$	-0.2 ± 0.5
		0.0 ± 0.1

[a]Each ribonuclease was rotated using Euler angles to obtain six starting orientations. Two independent 2 ns simulations were run for each orientation. The binding energy reports on the average energy over the duration of a simulation, and its standard deviation arises from variation in the trajectory.

movement during the simulation, with larger variations reflecting a varied trajectory. Coarse-grained representations for the trajectories of simulations that result in bound and unbound ONC are shown in Figure 5 panels B and E, respectively. The bound trajectory remains in the areas that are most energetically favorable, as seen in Figure 5A. The unbound trajectory was started in a less energetically favorable area, where the binding free energy was insufficient to keep ONC on the membrane long enough for it to rotate to a more energetically favorable orientation. The two simulations starting from orientation $\theta = 270°$, $\psi = 90°$ also demonstrate this phenomenon. They both move away from the membrane due to a lack of favorable interactions. Nevertheless, in simulation 1, ONC does not rotate into a conformation that allows it to return to the membrane, whereas in simulation 2, ONC rotates so that its most favorable surface faces the membrane, ultimately enabling it to bind with an energy of −2 kcal/mol. In contrast to ONC, RNase A and RNase 1 bound to the membrane in 9 of the 12 trajectories. The energies are similar to those from the PB calculations, and the trajectory snapshots follow the energetics predicted by the PB calculations. Lastly, none of the proteins inserted into the membrane, though they remained close to the membrane according to the average predictive binding energy.

■ DISCUSSION

A major factor that limits the efficacy of many putative protein chemotherapeutic agents is their delivery to the cytosol.[50] Lacking a receptor, cytotoxic ribonucleases undergo endocytosis and escape from endosomes.[9] Here, we use a combination of experimental and computational techniques to compare and contrast the effect of electrostatics on the interaction of RNase 1, RNase A, and ONC with lipid bilayers.

Our data suggest that electrostatic forces are sufficient to cause a weak association of ONC with the cell surface, where the protein remains until internalized via bulk-rate endocytosis.[23] Although computational results predict a weak affinity for a negatively charged surface, ONC spent most of its simulation time associated with the surface. Because bulk endocytosis occurs constitutively, time spent near the cell surface is critical for internalization. We suggest that the low experimental rate of ONC cellular uptake[22,23] is explicable by its low binding energy combined with the lack of a cell-surface binding partner.

Comparing the cellular uptake to the calculated binding energies reveals unusual disparities for RNase A compared to ONC and RNase 1. Calculations predict that RNase A has a cell-surface affinity similar to that of ONC, yet RNase A is internalized by cells at a rate that is 10^2-fold greater than that of ONC.[23] The absence of heparan sulfate and chondroitin sulfate on the cell surface reduces the internalization rate of an RI-evasive variant of RNase A by 4-fold but does not affect that of ONC.[23] We propose that the presence of these and other cell-surface moieties with a specific affinity for RNase A, but not ONC, explains the discrepancy between predicted and experimental results. RNase A and RNase 1 display similar levels of cellular uptake[29] even though RNase 1 has a higher net charge (Figure 1), demonstrates a salt dependence in its membrane affinity (Figure 2), and has a much higher predicted binding free energy (Table 1). These data are consistent with RNase A having a greater affinity for specific cell-surface moieties than does RNase 1.

Poisson−Boltzmann calculations were used to predict the affinity of the three homologous cationic proteins for an anionic membrane. Although explicit lipid-based membrane simulations are becoming increasingly powerful,[51] computing the binding free energy of a protein to a multicomponent lipid bilayer with atomistic models remains as a significant challenge. Given the simplicity of the lipid bilayer model, which consists of an implicit solvent and a plane of negatively charged spheres above a low-

dielectric slab, its correspondence with experimental data is encouraging. The simplicity of the lipid bilayer model decreases computational cost compared to explicit lipid models. Most importantly, the PB calculations directly address the contribution of *electrostatics* to the binding affinity of the cationic proteins to an anionic membrane.

IMM1−GC simulation results were consistent with the PB calculations and with experimental results. They provided additional insight by clarifying the necessary strength of an interaction for a long-lasting stable interaction to occur in the protein−membrane complex and by showing that hydrophobic interactions are involved only minimally. The lack of ribonuclease penetration of the membrane suggests that, in contrast to cell-penetrating peptides,[45] ribonucleases require more than electrostatic or hydrophobic forces to penetrate a lipid bilayer. IMM1−GC simulations required far fewer computational resources compared to the PB calculations and provided additional information, making them an attractive option for identifying energetically favorable orientations of proteins at the membrane surface and for estimating the binding free energy. We propose that the results of IMM1−GC simulations could be refined further by explicit membrane simulations starting from the predicted binding orientations, though gaining quantitative insights requires novel simulation methods that allow an efficient sampling of local lipid (de)mixing upon protein binding.

Our future efforts will focus on identifying residues in pancreatic-type ribonucleases that mediate their affinity for those glycans that are upregulated in cancer cells.[32] Manipulations that enhance such interactions could increase the clinical utility of chemotherapeutic agents on the basis of RNase 1 and its homologues.

■ AUTHOR INFORMATION

Corresponding Author
*R. T. Raines: e-mail, rtraines@wisc.edu; phone, 608-262-8588; fax, 608-890-2583.

Notes
The authors declare no competing financial interest.

■ ACKNOWLEDGMENTS

■ REFERENCES

(1) Raines, R. T. (1998) Ribonuclease A. *Chem. Rev. 98*, 1045−1065.

(2) Marshall, G. R., Feng, J. A., and Kuster, D. J. (2008) Back to the future: Ribonuclease A. *Biopolymers 90*, 259−277.

(3) Cuchillo, C. M., Nogués, M. V., and Raines, R. T. (2011) Bovine pancreatic ribonuclease: Fifty years of the first enzymatic reaction mechanism. *Biochemistry 50*, 7835−7841.

(4) Benito, A., Ribó, M., and Vilanova, M. (2005) On the track of antitumor ribonucleases. *Mol. BioSyst. 1*, 294−302.

(5) Costanzi, J., Sidransky, D., Navon, A., and Goldsweig, H. (2005) Ribonucleases as a novel pro-apoptotic anticancer strategy: Review of the preclinical and clinical data for ranpirnase. *Cancer Invest. 23*, 643−650.

(6) Arnold, U., and Ulbrich-Hofmann, R. (2006) Natural and engineered ribonucleases as potential cancer therapeutics. *Biotechnol. Lett. 28*, 1615−1622.

(7) Lee, J. E., and Raines, R. T. (2008) Ribonucleases as novel chemotherapeutics: The ranpirnase example. *BioDrugs 22*, 53−58.

(8) Ardelt, W., Ardelt, B., and Darzynkiewicz, Z. (2009) Ribonucleases as potential modalities in anticancer therapy. *Eur. J. Pharmacol. 625*, 181−189.

(9) Rutkoski, T. J., and Raines, R. T. (2008) Evasion of ribonuclease inhibitor as a determinant of ribonuclease cytotoxicity. *Curr. Pharm. Biotechnol. 9*, 185−189.

(10) Lomax, J. E., Eller, C. H., and Raines, R. T. (2012) Rational design and evaluation of mammalian ribonuclease cytotoxins. *Methods Enzymol. 502*, 273−290.

(11) Vasandani, V. M., Wu, Y.-N., Mikulski, S. M., Youle, R. J., and Sung, C. (1996) Molecular determinants in the plasma clearance and tissue distribution of ribonucleases of the ribonuclease A superfamily. *Cancer Res. 56*, 4180−4186.

(12) Dickson, K. A., Haigis, M. C., and Raines, R. T. (2005) Ribonuclease inhibitor: Structure and function. *Prog. Nucleic Acid Res. Mol. Biol. 80*, 349−374.

(13) Turcotte, R. F., and Raines, R. T. (2008) Interaction of onconase with the human ribonuclease inhibitor protein. *Biochem. Biophys. Res. Commun. 377*, 512−514.

(14) Lee, F. S., Shapiro, R., and Vallee, B. L. (1989) Tight-binding inhibition of angiogenin and ribonuclease A by placental ribonuclease inhibitor. *Biochemistry 28*, 225−230.

(15) Johnson, R. J., McCoy, J. G., Bingman, C. A., Phillips, G. N., Jr., and Raines, R. T. (2007) Inhibition of human pancreatic ribonuclease by the human ribonuclease inhibitor protein. *J. Mol. Biol. 367*, 434−449.

(16) Leland, P. A., Schultz, L. W., Kim, B.-M., and Raines, R. T. (1998) Ribonuclease A variants with potent cytotoxic activity. *Proc. Natl. Acad. Sci. U. S. A. 95*, 10407−10412.

(17) Leland, P. A., Staniszewski, K. E., Kim, B.-M., and Raines, R. T. (2001) Endowing human pancreatic ribonuclease with toxicity for cancer cells. *J. Biol. Chem. 276*, 43095−43102.

(18) Rutkoski, T. J., Kurten, E. L., Mitchell, J. C., and Raines, R. T. (2005) Disruption of shape-complementarity markers to create cytotoxic variants of ribonuclease A. *J. Mol. Biol. 354*, 41−54.

(19) Saxena, S. K., Rybak, S. M., Winkler, G., Meade, H. M., McGray, P., Youle, R. J., and Ackerman, E. J. (1991) Comparison of RNases and toxins upon injection into *Xenopus* oocytes. *J. Biol. Chem. 266*, 21208−21214.

(20) Wu, Y., Mikulski, S. M., Ardelt, W., Rybak, S. M., and Youle, R. J. (1993) A cytotoxic ribonuclease. Study of the mechanism of onconase cytotoxicity. *J. Biol. Chem. 268*, 10686−10693.

(21) Haigis, M. C., and Raines, R. T. (2003) Secretory ribonucleases are internalized by a dynamin-independent endocytic pathway. *J. Cell Sci. 116*, 313−324.

(22) Turcotte, R. F., Lavis, L. D., and Raines, R. T. (2009) Onconase cytotoxicity relies on the distribution of its positive charge. *FEBS J. 276*, 3846−3857.

(23) Chao, T.-Y., Lavis, L. D., and Raines, R. T. (2010) Cellular uptake of ribonuclease A relies on anionic glycans. *Biochemistry 49*, 10666−10673.

(24) Chao, T.-Y., and Raines, R. T. (2011) Mechanism of ribonuclease A endocytosis: Analogies to cell-penetrating peptides. *Biochemistry 50*, 8374−8382.

(25) Suzuki, M., Saxena, S. K., Boix, E., Prill, R. J., Vasandani, V. M., Ladner, J. E., Sung, C., and Youle, R. J. (1999) Engineering receptor-mediated cytotoxicity into human ribonucleases by steric blockage of inhibitor interaction. *Nat. Biotechnol. 17*, 265−270.

(26) Futami, J., Maeda, T., Kitazoe, M., Nukui, E., Tada, H., Seno, M., Kosaka, M., and Yamada, H. (2001) Preparation of potent cytotoxic ribonucleases by cationization: Enhanced cellular uptake and decreased interaction with ribonuclease inhibitor by chemical modification of carboxyl groups. *Biochemistry 26*, 7518−7524.

(27) Fuchs, S. M., Rutkoski, T. J., Kung, V. M., Groeschl, R. T., and Raines, R. T. (2007) Increasing the potency of a cytotoxin with an arginine graft. *Protein Eng., Des. Sel. 20*, 505−509.

(28) Futami, J., and Yamada, H. (2008) Design of cytotoxic ribonucleases by cationization to enhance intracellular protein delivery. *Curr. Pharm. Biotechnol. 9*, 180−184.

(29) Johnson, R. J., Chao, T.-Y., Lavis, L. D., and Raines, R. T. (2007) Cytotoxic ribonucleases: The dichotomy of Coulombic forces. *Biochemistry 46*, 10308−10316.

(30) Slivinsky, G. G., Hymer, W. C., Bauer, J., and Morrison, D. R. (1997) Cellular electrophoretic mobility data: A first approach to a database. *Electrophoresis 18*, 1109−1119.

(31) Ran, S., Downes, A., and Thorpe, P. E. (2002) Increased exposure of anionic phospholipids on the surface of tumor blood vessels. *Cancer Res. 62*, 6132−6140.

(32) Dube, D. H., and Bertozzi, C. R. (2005) Glycans in cancer and inflammation—potential for therapeutics and diagnostics. *Nat. Rev. Drug Discovery 4*, 477−488.

(33) Leich, F., Stohr, N., Rietz, A., Ulbrich-Hofmann, R., and Arnold, U. (2007) Endocytotic internalization as a crucial factor for the cytotoxicity of ribonucleases. *J. Biol. Chem. 282*, 27640−27646.

(34) Chao, T.-Y., and Raines, R. T. (2013) Fluorogenic label to quantify the cytosolic delivery of macromolecules. *Mol. BioSyst. 9*, 339−342.

(35) Rodriguez, M., Torrent, G., Bosch, M., Rayne, F., Dubremetz, J.-F., Ribó, M., Benito, A., Vilanova, M., and Beaumelle, B. (2007) Intracellular pathway of Onconase that enables its delivery to the cytosol. *J. Cell Sci. 120*, 1405−1411.

(36) Notomista, E., Mancheño, J. M., Crescenzi, O., Di Donato, A., Gavilanes, J., and D'Alessio, G. (2006) The role of electrostatic interactions in the antitumor activity of dimeric RNases. *FEBS J. 273*, 3687−3697.

(37) Talasaz, A., and Davis, R. (2006) Prediction of protein orientation upon immobilization on biological and nonbiological surfaces. *Proc. Natl. Acad. Sci. U. S. A. 103*, 14773−14778.

(38) Lavis, L. D., Chao, T.-Y., and Raines, R. T. (2006) Fluorogenic label for biomolecular imaging. *ACS Chem. Biol. 1*, 252−260.

(39) Baker, N. A., Sept, D., Joseph, S., Holst, M. J., and McCammon, J. A. (2001) Electrostatics of nanosystems: application to microtubules and the ribosome. *Proc. Natl. Acad. Sci. U. S. A. 98*, 10037−10041.

(40) Berisio, R., Sica, F., Lamzin, V. S., Wilson, K. S., Zagari, A., and Mazzarella, L. (2002) Atomic resolution structures of ribonuclease A at six pH values. *Acta Crystallogr., Sect. D 58*, 441−450.

(41) Mosimann, S. C., Ardelt, W., and James, M. N. G. (1994) Refined 1.7 Å X-ray crystallographic structure of P-30 protein, an amphibian ribonuclease with anti-tumor activity. *J. Mol. Biol. 236*, 1141−1153.

(42) MacKerell, A. D., Bashford, D., Bellott, M., Dunbrack, R. L., Evanseck, J. D., Field, M. J., Fischer, S., Gao, J., Guo, H., Ha, S., Joseph-McCarthy, D., Kuchnir, L., Kuczera, K., Lau, F. T. K., Mattos, C., Michnick, S., Ngo, T., Nguyen, D. T., Prodhom, B., Reiher, W. E., Roux, B., Schlenkrich, M., Smith, J. C., Stote, R., Straub, J., Watanabe, M., Wiorkiewicz-Kuczera, J., Yin, D., and Karplus, M. (1998) All-atom empirical potential for molecular modeling and dynamics studies of proteins. *J. Phys. Chem. B 102*, 3586−3616.

(43) Dolinsky, T. J., Nielsen, J. E., McCammon, J. A., and Baker, N. A. (2004) PDB2PQR: an automated pipeline for the setup, execution, and analysis of Poisson-Boltzmann electrostatics calculations. *Nucleic Acids Res. 32*, W665−W667.

(44) Dolinsky, T. J., Czodrowski, P., Li, H., Nielsen, J. E., Jensen, J. H., Klebe, G., and Baker, N. A. (2007) PDB2PQR: Expanding and upgrading automated preparation of biomolecular structures for molecular simulations. *Nucleic Acids Res. 35*, W522−W525.

(45) Lazaridis, T. (2005) Implicit solvent simulations of peptide interactions with anionic lipid membranes. *Proteins 58*, 518−527.

(46) Lazaridis, T., and Karplus, M. (1999) Effective energy function for proteins in solution. *Proteins 35*, 133−152.

(47) McLaughlin, S. (1989) The electrostatic properties of membranes. *Annu. Rev. Biophys. Biophys. Chem. 18*, 113−136.

(48) Brooks, B. R., Bruccoleri, R. E., Olafson, B. D., States, D. J., Swaminathan, S., and Karplus, M. (1983) CHARMM: A program for macromolecular energy, minimization, and dynamics calculations. *J. Comput. Chem. 4*, 187−217.

(49) Kelemen, B. R., Klink, T. A., Behlke, M. A., Eubanks, S. R., Leland, P. A., and Raines, R. T. (1999) Hypersensitive substrate for ribonucleases. *Nucleic Acids Res. 27*, 3696−3701.

(50) Arnold, U. (2008) Aspects of the cytotoxic action of ribonucleases. *Curr. Pharm. Biotechnol. 9*, 161−168.

(51) Khalili-Araghi, F., Gumbart, J., Wen, P. C., Sotomayor, M., Tajkhorshid, E., and Schulten, K. (2009) Molecular dynamics simulations of membrane channels and transporters. *Curr. Opin. Struct. Biol. 19*, 128−137.